Stereoscopic study of angle-dependent interlayer magnetoresistance in the organic conductor κ-(BEDT-TTF)$_2$Cu(NCS)$_2$

W. Kang,[1,*] Y. J. Jo,[1] D. Y. Noh,[2] K. I. Son,[2] and Ok-Hee Chung[3]
[1]*Department of Physics, Ewha University, Seoul 120-750, South Korea*
[2]*Department of Chemistry, Seoul Women's University, Seoul 139-774, South Korea*
[3]*Department of Physics, Sunchon University, Sunchon 540-742, South Korea*
(Received 20 April 2009; revised manuscript received 20 July 2009; published 1 October 2009)

We stereoscopically studied the angle-dependent interlayer magnetoresistance $R_{zz}(\theta,\phi)$ of the organic conductor κ-(BEDT-TTF)$_2$Cu(NCS)$_2$. A pressure of 7 kbar was applied to render the sample fully metallic. The stereoscopic view enables us to distinguish between quasi-one-dimensional (Q1D) and quasi-two-dimensional (Q2D) types of mixed angular magnetoresistance oscillations. A crossover between Q1D features and Q2D features is observed at $\phi \sim 35°$ when the field rotates in the conducting plane. While the coherence peak in the Q1D region has a constant angular width, 1.4°, the width of the humplike peak in the Q2D region grows with inverse cos ϕ dependence up to 25°. In addition, differences of the ϕ-dependence of $R_{zz}^{\theta=0}$ and of its temperature dependence support the crossover behavior between Q1D and Q2D dominance.

DOI: 10.1103/PhysRevB.80.155102 PACS number(s): 71.18.+y, 72.15.Gd, 74.70.Kn

I. INTRODUCTION

Coherence of interlayer transport is one of the most fundamental concepts for understanding the electronic structure of quasi-two-dimensional (Q2D) compounds such as "high-T_c" cuprates, layered ruthenates, and crystalline organic metals.[1] Only when the interlayer charge transfer is coherent, can the Fermi surface (FS) be defined as three-dimensional and extended in the interlayer direction. Beats in magnetic oscillations and a coherence peak at the conducting layer in the angle-dependent interlayer magnetoresistance are regarded as evidences of interlayer coherence in Q2D systems. In the case of quasi-one-dimensional (Q1D) conductors, a coherence peak can also be apparent depending upon the extent of the warping of the open FS. Although the electron trajectories are different between Q1D and Q2D systems, the interlayer dispersion plays a major role in determining the coherence peak features. In particular, studies of the coherence peak and of angular magnetoresistance oscillations (AMRO) are very attractive in some organic compounds such as κ-(BEDT-TTF)$_2$Cu(NCS)$_2$ and α-(BEDT-TTF)2KHg(SCN)4 [BEDT-TTF: bisethylenedithiotetrathiafulvalne] where Q1D and Q2D FSs coexist, because of how the two FSs contribute to angular resonance effects and interfere with each other.[2]

κ-(BEDT-TTF)$_2$Cu(NCS)$_2$ is one of the most characterized compounds among the BEDT-TTF based organic conductors.[3] A unit cell of κ-(BEDT-TTF)$_2$Cu(NCS)$_2$ crystal contains two dimers, therefore, two holes. The unperturbed FS in the layer, roughly circular and having the same area as the first Brillouin zone (FBZ),[4] cuts the rectangular FBZ boundaries on its long side. Periodic lattice potential opens gaps at the zone boundaries and splits the FS into a pair of Q1D electronic sheets and a Q2D hole pocket as shown in Fig. 1(a).[4–7] The FS topology of this compound is well verified by experimental observations of the Shubnikov-de Haas (SdH) and de Haas-van Alphen effects[4,5,8] and AMRO.[9] In previous studies, coherence peaks were observed[2] but beats of quantum oscillations were not found. Coherence peaks from Q1D and Q2D FS sections were discussed in light of 2D tight binding energy dispersion.[2]

There are certain traits to assure the dimensionality of the system in AMRO. The Kartsovnik-Kajita-Yamaji (KKY) oscillations from a Q2D FS appear as a series of resistance *peaks* of which the cotangents of the elevation angle from the conducting plane are linear to integer indices.[10–12] Angular positions of the KKY peaks (θ_N) oscillate on azimuthal rotations.[13] In contrast, the prominent angular oscillatory effect from the Q1D FS are the Lebed resonances in which the cotangents of the elevation angles of the resistance *dips* are linear to integer indices.[14] The angular positions of the dips ($\theta_{p/q}$) converge to zero as the rotation plane approaches the most conducting axis.[15] In addition, inherent Q1D features such as Danner-Kang-Chaikin (DKC) oscillations, an interlayer coherence peak,[16] and the third angular effect[17] appear as the field direction approaches the most conducting axis.[18] When Q1D and Q2D FSs coexist as in the title compound, the aforementioned AMRO are mixed and inseparable in usual rotation measurements.

A stereoscopic study of the angular magnetoresistance (AMR) with the 4π full rotation of the magnetic field is a solution to clarify each type of the mixed AMRO and the origin of the in-plane coherence peaks. In order to investigate the fine details of FS topology using a 14 T superconducting magnet, we applied a hydrostatic pressure of 7 kbar to render the sample fully metallic. The superconducting state is completely suppressed at 5 kbar[8] and the electronic structure of the Q1D and Q2D FSs is almost unchanged up to 7.5 kbar.[19]

We measured interlayer resistance $R_{zz}(\theta,\phi)$ in the angular range of $-66° < \phi < +174°$ and $-90° < \theta < +90°$, where ϕ and θ denote the azimuthal and elevation angles of the magnetic field direction, as depicted in Fig. 1(b). Considering the inversion symmetry of the crystal, the above range covers the totality of 4π directions of the field. This stereoscopic study of the AMR allows us to distinguish between the Q1D and the Q2D types in the entangled AMRO. When the field lies in the conducting plane, the ϕ region where the Q1D

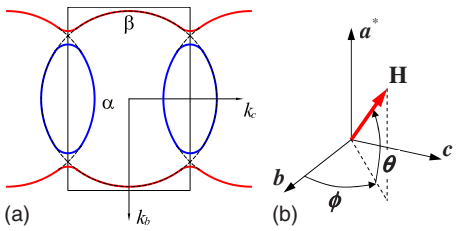

FIG. 1. (Color online) (a) Schematic diagram of the Fermi surfaces of κ-(BEDT-TTF)$_2$Cu(NCS)$_2$ on the k_bk_c-plane. The elliptic orbits represent the Q2D closed (α) orbits and the horizontally undulated orbits form the Q1D open orbits. In a sufficiently large field, electrons overcome the gap between two orbits and form large circular magnetic breakdown (β) orbits. The size of closed orbits and the undulation of open orbits are exaggerated for clarity. The rectangle is the first Brillouin zone in the k_bk_c plane. (b) Definition of the elevation angle θ and the azimuthal angle ϕ of a magnetic field in the sample.

features only appear is separated from the Q2D features dominant region. The coherence peak in the Q2D dominant region is contrary to that in typical Q2D systems,[20] and unusually large and wide. Additional indication for the Q1D to Q2D crossover appeared as the curvature change in $R_{zz}^{\theta=0}(\phi)$ and in $R_{zz}^{\theta=0}(T)$.

II. EXPERIMENTS

κ-(BEDT-TTF)$_2$Cu(NCS)$_2$ single crystals were grown with a typical electrochemical method.[3] The single crystals have a well-defined hexagonal shape and the dimension of the crystal used here is $0.8\times0.6\times0.1$ mm^3. Electrical contacts were made with 20 μm annealed gold wires using carbon paste. Interlayer resistance was measured along the crystallographic a^* axis with the standard four-wire *ac* technique. An *ac* current between 10 and 100 μA was used and the absence of nonlinear effect was assured. Pressure was applied in a miniature BeCu cell at room temperature with Daphne 7373 oil as pressure transmitting medium.[21] The pressure at low temperature was 7 kbar, determined from the shift in the superconductivity transition temperature of pure tin (Sn) element embedded next to the samples.[22] In zero-field cooling, R_{zz} decreases monotonously over the whole temperature range without suffering any jump [Fig. 2(a)]. A two-axis rotator probe was used to rotate the pressure cell in a 14 T superconducting magnet. Since the samples under 7 kbar remain metallic at low temperature,[8,23] the involvement of vortex dynamics is completely excluded.[24]

III. RESULTS AND DISCUSSION

Because of the platelike shape of the crystal, the a^* direction perpendicular to the conducting layer could be unambiguously determined prior to the experiments. The *b* and *c* axes can be determined from the shape of crystals and confirmed, *a posteriori*, from experimental data. The sharpness of the oscillatory features such as the Q1D coherence peak

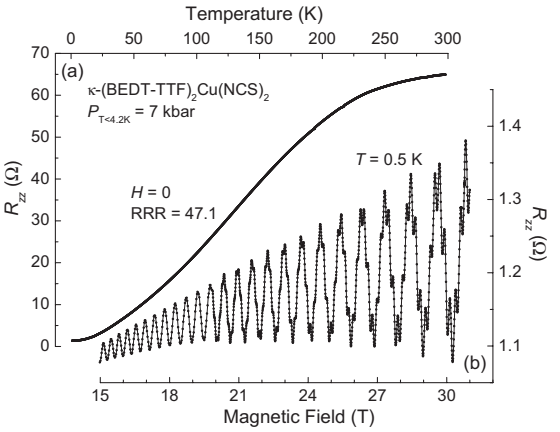

FIG. 2. General characteristics of the κ-(BEDT-TTF)$_2$Cu(NCS)$_2$ at 7 kbar. (a) Temperature dependence of the interlayer resistance in zero field. The sample did not suffer any minor resistance jump and have a residual resistance ratio of 47. (b) $R_{zz}(H)$ at T=0.5 K shows both the primary (H_α) and the magnetic breakdown (H_β) SdH oscillations at high magnetic fields. The field direction is 4.5° apart from the a^* direction in the a^*c plane.

and the SdH oscillations excludes spurious effects due to sample twinning or pressure inhomogeneity. A separate measurement up to 31 T confirmed that the primary SdH oscillation frequency H_α is 712 ± 1 T and the breakdown frequency H_β is 4055 ± 3 T for the magnetic field direction parallel to the a^* direction [Fig. 2(b)]. These frequencies are consistent with previous results by Caulfield *et al.*[8]

Figure 3 shows the θ-dependence of AMR, $R_{zz}(\theta)$, for several fixed ϕ values. $R_{zz}^{\phi_{\text{fixed}}}(\theta)$ is quite complicated because contributions from the Q1D and Q2D FSs are superimposed. When $|\phi|<30°$ and $|\theta|<20°$, meaning the field is aligned near the *b* axis, the coherence peak and the DKC oscillations make obvious that the Q1D features only are present although the similar Q2D features are expected due to closed motions on the corrugated Q2D FS at this field direction. Therefore, the angular region of $|\phi|<30°$ and $|\theta|<20°$ is termed the Q1D dominant region. On the other hand, the AMRO at larger ϕ appears to combine KKY oscillations with Lebed oscillations. The mixture of two resonant features can be classified by the stereoscopic presentation of the AMR since their ϕ-dependence is substantially different.

Various stereoscopic views of $R_{zz}(\theta,\phi)$ are presented in Fig. 4. Figures 4(a) and 4(d) are the $R_{zz}(\theta,\phi)$ viewed from the (121) and (100) directions, respectively. Resistance is zero at the origin and the distance from the origin to a point on the surface is proportional to the resistance when the magnetic field aligns to that direction. Conductance ($\sim1/R_{zz}$) views from (010) and (001) directions are presented in Figs. 4(b) and 4(c). Finer features in Fig. 4 will be discussed in detail hereafter.

When the magnetic field is aligned to near the least conducting axis, the $R_{zz}(\theta,\phi)$ shows densely spaced concentric ridges centered on the a^* direction. As proved in Fig. 5, they are periodic to $(H\sin\theta)^{-1}$ with frequency 710 T, verifying as the SdH oscillations from the α orbits of the FS.[5,8]

On the other hand, when the field direction is near parallel to the *b* axis across to the Q1D FS in *k* space, a rhombus is

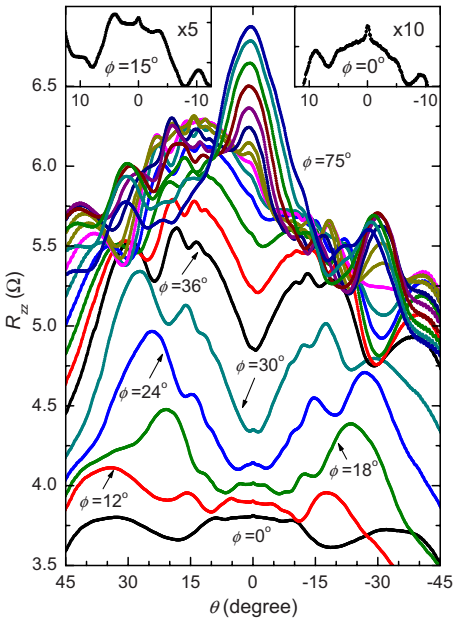

FIG. 3. (Color online) Angular magnetoresistance $R_{zz}(\theta)$ for fixed ϕ in $0° < \phi < 75°$ at $T=1.6$ K, $H=14$ T, and $P=7$ kbar. For $36° < \phi < 75°$, traces are in 3° steps. The coherence peak with a width of ~1.4° at $\phi < 30°$ is from the Q1D FS. A new peak from the Q2D FS begins to appear around 36° and rapidly grows to a prominent hump as ϕ increases toward 90°. The width of the peak $2\Delta_\theta$ at $\phi > 75°$ is about 25°. The insets show detailed views of the Q1D coherence peak at $\phi=0°$ and 15°.

formed around the b axis. It ranges from $\phi \simeq -33°$ to +33° and from $\theta \simeq -10°$ to +10° as shown in Fig. 4(a). The boundary ridge of the rhombus is formed by the local maxima of the DKC oscillations as shown in Fig. 3. There are a few weak secondary peaks inside the rhombus. The coherence peak at $\theta=0$ for $|\phi| < 30°$ appears as a narrow ridge along the horizontal axis inside of the rhombus. The coherence peak keeps the same height and a constant angular width of

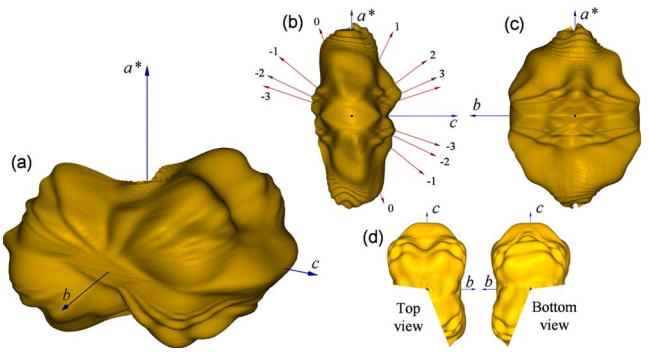

FIG. 4. (Color online) (a) Stereoscopic view from the (121) of the AMR $R_{zz}(\theta,\phi)$ of κ-(BEDT-TTF)$_2$Cu(NCS)$_2$ at $T=1.6$ K, $H=14$ T, and $P=7$ kbar. The resistance is plotted linear to the radial distance from the origin to a point on the surface to which the field aligns. Conductance ($\sim 1/R_{zz}$) views (b) from the (010) and (c) from the (001) directions. Arrows and numbers represent the primary Lebed resonance angles with their indices. (d) Top (100) and bottom ($\bar{1}00$) views of the AMR.

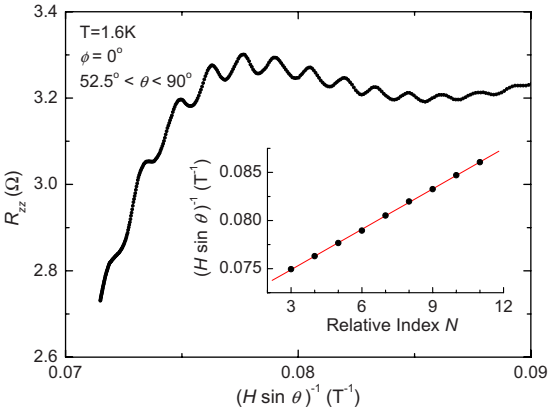

FIG. 5. (Color online) $R_{zz}(\theta)$ versus $(H \sin\theta)^{-1}$, which shows densely spaced oscillations centered on the a^* direction are periodic to $(H \sin\theta)^{-1}$. The inset confirms the positions of resistance maxima are periodic to $(H \sin\theta)^{-1}$ with a frequency of 710 T.

$1.4 \pm 0.2°$. It is reasonable to attribute the coherence peak to the Q1D FS likewise the DKC oscillations although interlayer warping on both the Q1D FS and the Q2D FS can contribute to the coherence peak at the b axis.

Beyond the horizontal rhombus edge ($|\phi| > 33°$), a broad dip develops in the $R_{zz}(\theta)$ (Fig. 3), which is already seen in typical Q1D systems.[18] However, a new kind of small peak sprouts from near the minimum. As ϕ increases toward 90°, while the broad dip reduces in size and vanishes above 54°, the new small peak grows larger to a prominent hump as shown in Figs. 3 and 4(a). This humplike peak along the c axis is incomparably different from the coherence peak at $|\phi| < 33°$.

To characterize the two peaks, the ϕ-dependence of the angular width of two kinds of peaks is plotted in Fig. 6. The angular width of the coherence peak at $|\phi| < 33°$ is observed as $1.4 \pm 0.2°$ and ϕ-independent. On the other hand, the width $2\Delta_\theta$ of the new peak varies with the inverse of cos ϕ at $\phi > 36°$ and saturates to about 25° as ϕ is above 75°,

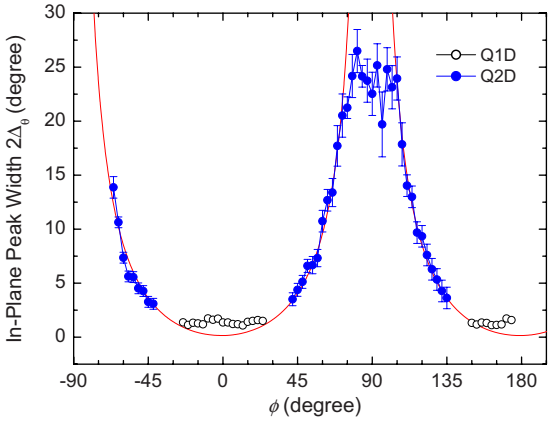

FIG. 6. (Color online) Angular width $2\Delta_\theta$ of coherence peaks versus azimuthal angle ϕ. Open circles are from the Q1D FS and filled circles from the Q2D FS. The regions without data points correspond to the angular interval where the dominant FS changes. Lines of an inverse cosine function of ϕ fit to the Q2D data for ϕ more than 15° apart from the $\pm c$ axis.

approaching the c axis. According to Goddard *et al.* reporting on the interlayer coherence peaks in κ-(BEDT-TTF)$_2$Cu(NCS)$_2$ at ambient pressure and at high field of 42 T, there are two branches of the peak resulting from the closed orbital motions on the Q1D and Q2D FSs.[9] The angular width varies sinusoidally between 0.4 and 1.2° and has a minimum at ϕ=90°. Our observation of two distinct coherence peaks at different angular regions is in contrast to the previous report. The humplike peak at c direction and inverse cos ϕ dependence of its angular width have never been reported. For the field nearly parallel to the c axis, closed orbital motions are on the Q2D FS but only open trajectories on the Q1D FS. Therefore, the bulged peak near the c axis at $\phi>35°$ should be attributed to the closed motion on the corrugated cylindrical Q2D FS while the ϕ-independent coherence peak along the b direction at $\phi<35°$ originated from the closed motion on the warped Q1D FS. Pressure of 7 kbar can increase interlayer corrugation of the Q2D FS and result in this anomalous peak. However, the Q1D coherence peak at the b axis exhibits almost the same behavior of that at the ambient pressure. It suggest that the interlayer warping of the Q1D FS remains almost unchanged at 7 kbar. Although the applied pressure can significantly increase the dimensionality of the Q2D FS, the inverse cos ϕ dependence of its width is not explainable with known Q2D band models.

In highly anisotropic materials, the angular width of the coherent peak can be roughly approximated by $\sim v_\perp/v_\parallel$ where the out-of-plane velocity of quasiparticles, $v_\perp$, remains constant but the in-plane velocity, $v_\parallel$, varies with ϕ. The dispersion relation of energy and anisotropic in-plane FS parameters of elliptical Q2D will determine the ϕ-dependence of the angular width of the peak. However, neither the prevailing size nor $1/\cos\phi$ dependence of peak width is explainable with typical anisotropic Q2D energy model and homogeneous interlayer transfer integral.

Confirming their topological origin, the angular width of both the Q1D peak and the Q2D peak does not depend markedly on temperature or on magnetic field. The Q2D peak is particularly robust as it is visible in fields as low as 4 T and at temperatures as high as 30 K as shown in Fig. 7. However, neither the ϕ dependence nor the large width coincides with the topological origin from the FS.

Inside of the rhombus around the b axis in Fig. 4, R_{zz} is mostly flat, i.e., $R_{zz}\cos\alpha$=constant, where the angle α stands for the polar angle measured from the b axis. $R_{zz}^{\theta=0}(\phi)$ in κ-(BEDT-TTF)$_2$Cu(NCS)$_2$ shows the inverse cosine dependence of ϕ without the third angular effect in contrast to that in typical Q1D TMTSF compounds. Although the third angular effect is absent, the coherence peak with DKC oscillations, and the rhombus pattern around the b axis indicate that Q1D effect is dominant in this angular regime. As the in-plane field direction reaches above 35° from the b axis where the Q2D coherence peak begins to grow the inverse cos ϕ dependence of $R_{zz}^{\theta=0}(\phi)$ is no more valid. Therefore, the different ϕ-dependence in resistance above 35° may result from the system entering the Q2D regime from the Q1Ds.

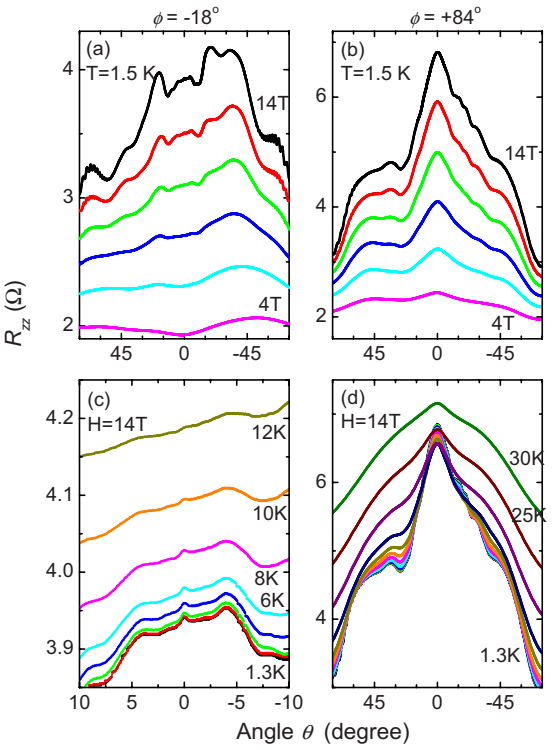

FIG. 7. (Color online) Magnetic field and temperature dependence of coherence peaks at ϕ=−18° [(a) and (c)] and at ϕ=84° [(b) and (d)].

Another interesting finding is that temperature dependence of $R_{zz}^{\theta=0}$ exhibits quite different behavior depending on which angular regime the system is in. $R_{zz}^{\theta=0}(T)$ for four azimuthal angles (ϕ=−40, −19, 41, and 83°) in the in-plane field, 14 T, is plotted in Fig. 8. While the $R_{zz}^{\theta=0}(T)$ at ϕ =−19° decreases monotonically down to 1.5 K, $R_{zz}^{\theta=0}(T)$ at ϕ=41° shows a small increase at ~15 K. As the field direction approaches the c axis, the upturn in the resistance below 15 K becomes more manifest. The ϕ angle where the temperature dependence of $R_{zz}^{\theta=0}$ becomes different is around 40° which corresponds to the edge of the rhombus. In addition to the dissimilarity of the coherence peaks and of the ϕ-dependence of $R_{zz}^{\theta=0}$ between the two angular regions, the different temperature dependence of $R_{zz}^{\theta=0}$ can also be due to the dimensional crossover between the Q1D and Q2D regions.[25]

Next, the fine oscillation features in the tilted magnetic field will be classified. Returning to Fig. 4, radially converging resistance valleys toward the b axis at outside of the rhombus in Fig. 4(a) are identified as Lebed resonances corresponding to radial ridges in the conductance view from (010) in Fig. 4(b). Angular positions of the conductance ridges corresponds to Lebed magic angles obtained from the crystal parameters at low temperature and high pressure.[19] Primary Lebed angles are indicated by arrow lines in Fig. 4(b).

The conductance view from the (001) direction [Fig. 4(c)] exhibits that dark valleys running diagonally from the c axis intersect and modulate the Lebed resonance ridges. Resonant angles (θ_N) for these valleys are substantially larger in the

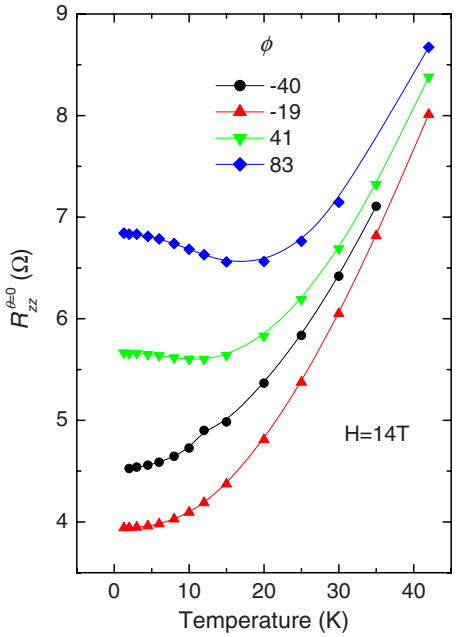

FIG. 8. (Color online) Temperature dependence of $R_{zz}^{\theta=0}$ is measured for several fixed ϕ's. T-dependence is quite different between two regimes (see the text).

a^*b plane than in the a^*c plane from the Q2D FS pocket longer along the b direction. As traces of the conductance valleys do not converge to the bc plane, they are interpreted as KKY resonances.

Equirectangular projection of $R_{zz}(\theta,\phi)$ and the second derivative of R_{zz} in Figs. 9(a) and 9(b) show the subtle relationship among the AMRO and how they evolve in the intermediate angular region. In Fig. 9(a), the resistance is represented on a logarithmic gray scale with a range of 2.5–7.0 Ω. Darker regions denote higher resistance. The bright lozenge around the b axis ($\phi=0$ and $\theta=0$) and bright arcs in Fig. 9(a) [dark ones in Fig. 9(b)] correspond to the DKC rhombus and Lebed resonance dips. In contrast to previous descriptions,[9] it is clearly seen that Lebed resonances, the primary Q1D feature, are continuous for whole ϕ-range. The black area around $\phi=90°$ and $\theta=0$ represents the resistance humplike peaks around the c axis in Fig. 3 and Fig. 4(a). The dark area between the bright diagonal lines corresponds to the KKY resonance peaks only visible when ϕ is above 30°. This figure clearly shows that two resonances develop simultaneously and interfere with each other, particularly in $|\theta|<45°$ and $30°<\phi<150°$. Both the SdH and the AMRO features are more clearly viewed in the second derivative, $d^2R_{zz}(\theta,\phi)/d\theta^2$. Overall equirectangular plot of the AMR is similar to the recent numerical calculation by Nowojewski *et al.* in the field regime of $B\sim B_0$, where B_0 is the magnetic breakdown field.[26] However, quantum oscillations due to the magnetic breakdown orbits did not appear at this field strength.[27]

In addition, the AMR behaves asymmetrically between the upper and the lower hemispheres in the plane normal to the b axis. While $R_{zz}^{\phi=90°}(\theta)$ shows monotonic collapse with elusive AMRO features in $0<\theta<90°$ (upper hemisphere view), it reveals the manifest angular oscillations added to

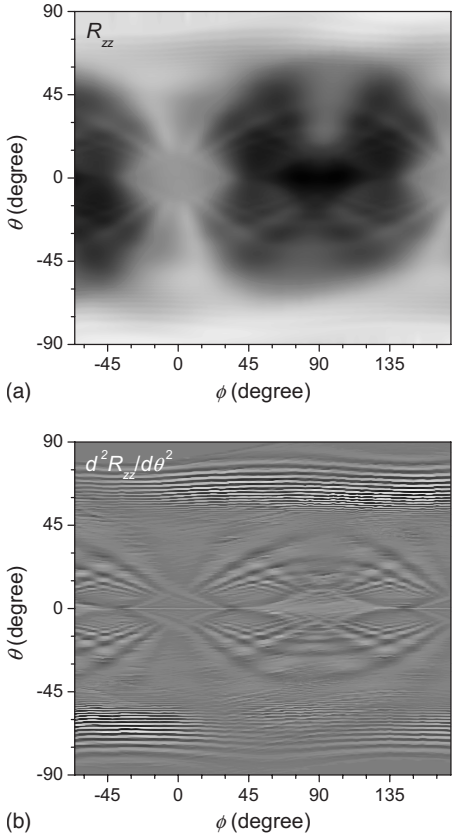

FIG. 9. (a) Equirectangular projection of $R_{zz}(\theta,\phi)$ of κ-(BEDT-TTF)$_2$Cu(NCS)$_2$ at 7 kbar, 14 T, and 1.6 K. The resistance is plotted on a logarithmic gray scale (2.5–7.0 Ω). The darker region represents the larger resistance. (b) The features are more clearly viewed in the second derivative, $d^2R_{zz}(\theta,\phi)/d\theta^2$.

the risen resistance in $-90°<\theta<0$ [lower hemisphere view in Fig. 4(d)]. The asymmetry in the a^*c plane is due to the monoclinic structure of the crystal. Although the oscillation features are faint along the resistance valley on the upper view, they are identified as the Lebed oscillations by equirectangular plot in Fig. 9 as well as the obvious ones on the lower view. However, this collapse is distinct from the collapse of the Lebed resonance in pure Q1D systems.[18]

Analysis of the AMRO together with the SdH oscillations at 7 kbar shows that the major axis of the α orbit is 1.98×10^9 m^{-1} long and the minor axis 1.10×10^9 m^{-1}, compared to 2.28×10^9 m^{-1} and 0.80×10^9 m^{-1} obtained at the ambient pressure.[9] The pressure effect on the Q2D FS is strongly anisotropic in the k_bk_c plane because the minor axis of Q2D FS increases while the major axis decreases with pressure. So, the cross section of the Q2D FS becomes less elliptic and the Q2D electronic structure becomes more isotropic. The SdH oscillation frequency of the α orbit, the cross section of the Q2D FS, increased by ~19% at 7 kbar, which is comparable to the previous reports.[8] The cross section of the Q2D FS is substantially enlarged while the area of the FBZ is increased by only 3–4%. This fact indicates that, unlike Q2D FS, Q1D FS remains almost unaffected at the pressure. However, how the pressure affect the third direction of the each FS and the interlayer transfer is still obscure.

IV. CONCLUSION

In summary, we studied the stereoscopic AMR of κ-(BEDT-TTF)$_2$Cu(NCS)$_2$ in the metallic state by applying a pressure of 7 kbar. Both the Lebed resonances and the KKY resonances superimposed over a wide range of field directions are distinguished by stereoscopic AMR measurements. Lebed features are most prominent in the overall AMRO while the KKY resonances intercept and modulate the Lebed AMRO. As for the coherence peak in in-plane magnetic fields, there is a crossover from the Q1D peak to the Q2D one. The width of the Q1D coherence peak remains constant within the rhombus around the b axis. That of the Q2D coherence peak follows an inverse cosine function of ϕ. It becomes anomalously large and saturates around 25° as the magnetic field approaches the c axis. In addition, the fact that the ϕ- and temperature dependences of $R_{zz}^{\theta=0}$ are quite different between two angular regions supports the dimensional crossover between Q1D and Q2D dominant regions.

ACKNOWLEDGMENTS

This work was supported by the Korea Science and Engineering Foundation (Grants No. R01-2007-000-20576-0, No. R11-2008-053-02002-0 for W.K., and No. R01-2007-000-11915-0 for O.H.C.). We thank K. Murata for making the Daphene 7373 oil available. The high field SdH oscillations were verified by using a 31 T resistive magnet at the National High Magnetic Field Laboratory, which is supported by NSF Cooperative Agreement No. DMR-0654118, by the State of Florida, and by the DOE.

*wkang@ewha.ac.kr

[1] J. Singleton, P. A. Goddard, A. Ardavan, A. I. Coldea, S. J. Blundell, R. D. McDonald, S. Tozer, and J. A. Schlueter, Phys. Rev. Lett. **99**, 027004 (2007).

[2] J. Singleton, P. A. Goddard, A. Ardavan, N. Harrison, S. J. Blundell, J. A. Schlueter, and A. M. Kini, Phys. Rev. Lett. **88**, 037001 (2002).

[3] H. Urayama, H. Yamochi, G. Saito, K. Nozawa, T. Sugano, M. Kinoshita, S. Sato, K. Oshima, A. Kawamoto, and J. Tanaka, Chem. Lett. **17**, 55 (1988).

[4] T. Sasaki, H. Sato, and N. Toyota, Solid State Commun. **76**, 507 (1990).

[5] K. Oshima, T. Mori, H. Inokuchi, H. Urayama, H. Yamochi, and G. Saito, Phys. Rev. B **38**, 938 (1988).

[6] H. Mori, S. Tanaka, M. Oshima, G. Saito, T. Mori, Y. Maruyama, and H. Inokuchi, Bull. Chem. Soc. Jpn. **63**, 2183 (1990).

[7] T. Sasaki, H. Sato, and N. Toyota, Physica C **185-189**, 2687 (1991).

[8] J. Caulfield, W. Lubczynski, F. L. Pratt, J. Singleton, D. Y. K. Ko, W. Hayes, M. Kurmoo, and P. Day, J. Phys.: Condens. Matter **6**, 2911 (1994).

[9] P. A. Goddard, S. J. Blundell, J. Singleton, R. D. McDonald, A. Ardavan, A. Narduzzo, J. A. Schlueter, A. M. Kini, and T. Sasaki, Phys. Rev. B **69**, 174509 (2004).

[10] M. V. Kartsovnik, P. A. Kononovich, V. N. Laukhin, and I. F. Schegolev, Pis'ma Zh. Eksp. Teor. Fiz. **48**, 498 (1988) [JETP Lett. **48**, 541 (1988)].

[11] K. Kajita, Y. Nishio, T. Takahashi, W. Sasaki, R. Kato, and H. Kobayashi, Solid State Commun. **70**, 1189 (1989).

[12] K. Yamaji, J. Phys. Soc. Jpn. **58**, 1520 (1989).

[13] The angular positions θ_N of the KKY resonance peaks are given as (Ref. 12) $ck_F \cot \theta_N = \pi(N-\frac{1}{4})-C$, where c is the distance between adjacent conducting planes, k_F is the wave vector whose projection is on the Fermi surface, and N is the index of resonance. C is a constant depending on the azimuthal angle.

[14] A. G. Lebed, Pis'ma Zh. Eksp. Teor. Fiz. **43**, 137 (1986) [JETP Lett. **43**, 174 (1986)].

[15] Lebed's original suggestion (Ref. 14) was extended to give the resonance angles $\theta_{p/q}$ for arbitrary azimuthal plane such as (Refs. 28 and 29) $\frac{B_y}{B_z} = \cot \theta_{p/q} \sin \phi = \frac{p}{q} \frac{b \sin \gamma}{c \sin \beta \sin \alpha^*} - \cot \alpha^*$ regardless of B_x. Here, b, c, β, γ, and α^* are lattice parameters, and p and q are small integers.

[16] G. M. Danner, W. Kang, and P. M. Chaikin, Phys. Rev. Lett. **72**, 3714 (1994).

[17] T. Osada, S. Kagoshima, and N. Miura, Phys. Rev. Lett. **77**, 5261 (1996).

[18] W. Kang, T. Osada, Y. J. Jo, and H. Kang, Phys. Rev. Lett. **99**, 017002 (2007).

[19] M. Rahal, D. Chasseau, J. Gaultier, L. Ducasse, M. Kurmoo, and P. Day, Acta Crystallogr., Sect. B: Struct. Sci. **53**, 159 (1997).

[20] M. V. Kartsovnik, V. N. Laukhin, S. I. Pesotskii, I. F. Schegolev, and V. M. Yakovenko, J. Phys. I **2**, 89 (1992).

[21] K. Murata, H. Yoshino, H. O. Yadav, Y. Honda, and N. Shirakawa, Rev. Sci. Instrum. **68**, 2490 (1997).

[22] L. D. Jennings and C. A. Swenson, Phys. Rev. **112**, 31 (1958).

[23] W. Kang, D. Jérome, C. Lenoir, and P. Batail, J. Phys.: Condens. Matter **2**, 1665 (1990).

[24] M. Chaparala, O. H. Chung, Z. F. Ren, M. White, P. Coppens, J. H. Wang, A. P. Hope, and M. J. Naughton, Phys. Rev. B **53**, 5818 (1996).

[25] A. G. Lebed, N. N. Bagmet, and M. J. Naughton, Phys. Rev. Lett. **93**, 157006 (2004).

[26] A. Nowojewski, P. A. Goddard, and S. J. Blundell, Phys. Rev. B **77**, 012402 (2008).

[27] A. F. Bangura, P. A. Goddard, J. Singleton, S. W. Tozer, A. I. Coldea, A. Ardavan, R. D. McDonald, S. J. Blundell, and J. A. Schlueter, Phys. Rev. B **76**, 052510 (2007).

[28] I. J. Lee and M. J. Naughton, Phys. Rev. B **57**, 7423 (1998).

[29] A. G. Lebed and M. J. Naughton, Phys. Rev. Lett. **91**, 187003 (2003).